# Comparison of the squared binary, sinusoidal pulse width modulation, and optimal pulse width modulation methods for three-dimensional shape measurement with projector defocusing

Yajun Wang and Song Zhang*

Department of Mechanical Engineering, Iowa State University, Ames, Iowa 50011, USA

*Corresponding author: song@iastate.edu

Received 22 August 2011; revised 7 November 2011; accepted 9 November 2011; posted 9 November 2011 (Doc. ID 153221); published 24 February 2012

This paper presents a comparative study on three sinusoidal fringe pattern generation techniques with projector defocusing: the squared binary defocusing method (SBM), the sinusoidal pulse width modulation (SPWM) technique, and the optimal pulse width modulation (OPWM) technique. Because the phase error will directly affect the measurement accuracy, the comparisons are all performed in the phase domain. We found that the OPWM almost always performs the best, and SPWM outperforms SBM to a great extent, while these three methods generate similar results under certain conditions. We will briefly explain the principle of each technique, describe the optimization procedures for each technique, and finally compare their performances through simulations and experiments. 

*OCIS codes:* 120.0120, 120.2650, 100.5070.

## 1. Introduction

Over the past decades, digital sinusoidal fringe projection techniques have been very successful in the field of 3D optical profilometry and applied to numerous application areas [1–3]. However, they still encounter challenges due to the speed limitation as well as the nonlinear gamma effect. Conventionally, the projector switching speed, which is typically less than 120 Hz, limits the measurement speed. However, studies, such as high-frequency vibration, require speed faster than 120 Hz. Furthermore, when a common digital projector is used, nonlinear gamma effect will introduce errors. And then gamma calibration is required. Numerous methods [4–9] have been proposed to reduce the measurement errors caused by the nonlinear gamma. Though successful, the residual errors are usually nonnegligible for high-precision measurement applications.

The recently proposed squared binary defocusing technique (SBM) [10] has demonstrated its potential to overcome the aforementioned limitations. However, it poses new challenges: (1) the error induced by high-order harmonics and (2) the smaller depth measurement range. Endeavors have been made to conquer these challenges: (1) Ayubi *et al.* proposed a technique called sinusoidal pulse width modulation (SPWM) [11], and (2) Wang and Zhang proposed a technique called optimal pulse width modulation (OPWM) [12]. The two methods have demonstrated their superiorities over the SBM under certain conditions, while having their own limitations. The square binary method is sensitive to defocusing effect. It can only give good results when the binary structures are properly defocused to sinusoidal

1559-128X/12/070861-12$15.00/0

ones. This means the depth range of measurement is pretty small when SBM is adopted. Both recently proposed SPWM and OPWM techniques have the ability to improve the SBM method. They can produce high-quality 3D shape measurement even when the defocusing degree is small, which means the depth range of measurement for these two methods is larger than that for the SBM. Since each method has its own merits and shortcomings, it would be of interest to present thorough comparisons to the society among the three methods: SBM, SPWM, and OPWM.

It is important to note that this paper examines the method differences from the *phase* perspective since the 3D shape measurement quality is mainly determined by the quality of phase data for fringe projection techniques. It is also important to note that it is almost impossible to compare these methods exhaustively in one paper due to the fact that there are numerous variables affecting the measurement quality. Therefore, we limit our paper to a few case studies that will provide sufficient critical characteristics of these methods which are vital for 3D shape measurement. Specifically, we will focus on analyzing the phase errors caused by the three methods under different conditions, and we will use a three-step phase-shifting algorithm with equal phase shifts to perform phase analysis for simplicity and speed. The phase error is obtained by taking the differences between the phase obtained from the defocusing methods and the phase from the traditional ideal sinusoidal fringe projection method. Since we are studying the phase error caused by defocusing, the amount of defocusing needs to be accounted for. This research will consider two representative scenarios: the nearly focused case and the significantly defocused case. Different breadths of fringe patterns will also be examined for comparisons. Both simulations and experimental results will be presented in this paper to demonstrate the differences among SBM, SPWM, and OPWM.

Section 2 will explain the principle of each technique. Section 3 will present an optimization strategy for each technique. Section 4 and Section 5 respectively show simulation and experimental results under optimal conditions, and finally Section 6 summarizes the paper.

## 2. Principle

### A. Three-Step Phase-Shifting Algorithm

Phase-shifting algorithms are widely used in optical metrology because of their measurement speed and accuracy [13]. Numerous phase-shifting algorithms have been developed including three step, four step, double three step, and five step. In this paper, we use a three-step phase-shifting algorithm with a phase shift of $2\pi/3$ for simplicity and speed. Three fringe images can be described as

$$I_1(x,y) = I'(x,y) + I'(x,y)\cos(\phi - 2\pi/3), \quad (1)$$

$$I_2(x,y) = I'(x,y) + I'(x,y)\cos(\phi), \quad (2)$$

$$I_3(x,y) = I'(x,y) + I'(x,y)\cos(\phi + 2\pi/3), \quad (3)$$

where $I'(x,y)$ is the average intensity, $I''(x,y)$ the intensity modulation, and $\phi(x,y)$ the phase to be solved. Solving these equations simultaneously leads to

$$\phi(x,y) = \tan^{-1}\left[\sqrt{3}(I_1 - I_3)/(2I_2 - I_1 - I_3)\right]. \quad (4)$$

Equation (4) provides the phase ranging $[-\pi, \pi)$ with $2\pi$ discontinuities.

### B. Squared Binary Method

Our recent study indicated that it is feasible to generate high-quality sinusoidal fringe patterns by properly defocusing squared binary structured patterns [10]. Therefore, instead of sending sinusoidal fringe images to a focused projector, sinusoidal fringe patterns can be generated by defocusing binary structured ones. Figure 1 illustrates projector defocusing at different degrees. In this experiment, the projector projects squared binary structured patterns onto a uniform white board where the camera focuses. The projector defocusing is realized by adjusting the focal length of the projector gradually from in focus to out of focus. This experiment shows that if projector is properly defocused, seemingly sinusoidal fringe patterns can be generated. However, the phase error will be significant if there is no error compensation and the projector is not properly defocused [14].

### C. Sinusoidal Pulse Width Modulation

Recently, Ayubi *et al.* proposed an interesting technique that can significantly reduce phase errors even when the projector is not defocused properly for SBM, which is known as the SPWM technique [11]. The SPWM is a well-studied technique in power electronics to generate sinusoidal signal in time by filtering the binary signals. In brief, to generate low frequency ($f_0$) sinusoidal fringe patterns, a higher-frequency $f_c$ triangular wave $S^m(f_c)$ is used to modulate the desired ideal sinusoidal signal $S^i(f_0)$:

$$S^m(f_c) = \begin{cases} 2f_c x - 2N & x \in [N/f_c, (2N+1)/(2f_c)) \\ -2f_c x + 2N + 2 & x \in [(2N+1)/(2f_c), (N+1)/f_c) \end{cases}, \quad (5)$$

$$S^i(f_0) = 0.5 + 0.5\cos(2\pi f_0 x). \quad (6)$$

Here $f_c > f_0$, and $N$ is an integer.

The modulated fringe pattern for each point can then be generated as follows:

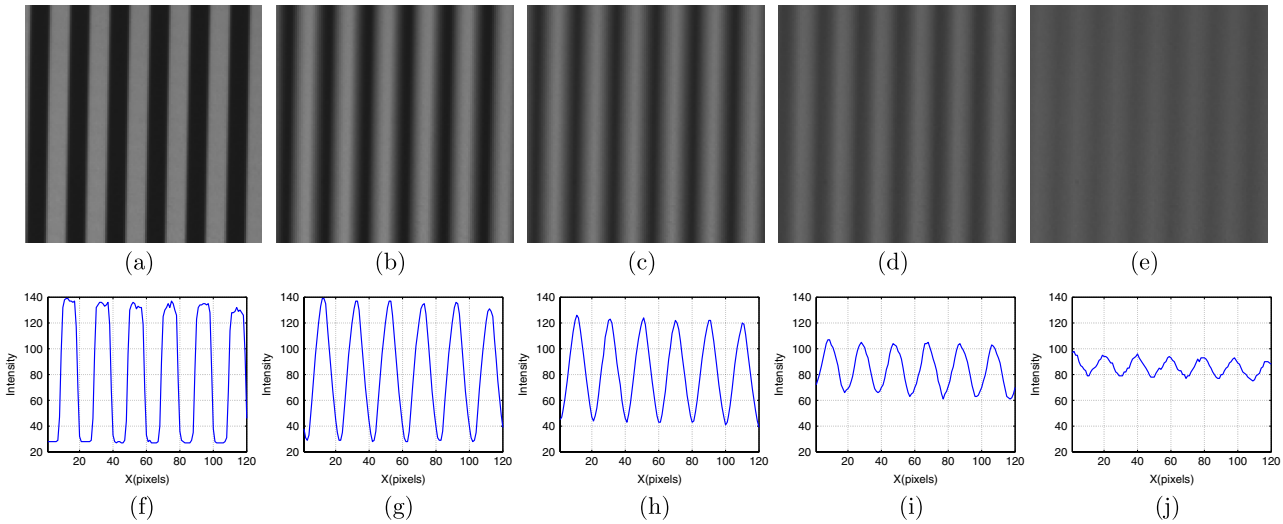


Fig. 1. (Color online) Influences of different defocusing degrees on the squared binary pattern. (a)–(e) show the patterns when the projector is nearly in focus to significantly defocused. (f)–(j) show the corresponding cross sections.

$$I^b(x,y) = \begin{cases} 1 & S^m(f_c) > S^i(f_0), \\ 0 & \text{otherwise} \end{cases}. \tag{7}$$

Figure 2 illustrates the SPWM pattern generation nature by modulating squared binary patterns with triangular waveform.

Defocusing is essential to suppress the high-order harmonics of the binary patterns while maintaining the fundamental frequency ($f_0$). The idea of SPWM is to shift the third and higher-order harmonics further away from the fundamental frequency so that they can be easier to be suppressed. Therefore, the modulated signal can then be converted to ideal sinusoidal signal by using a smaller size low-pass filter. In other words, the projector can be less defocused for sinusoidal fringe generation. By this means, the fringe contrast can be increased, and the depth measurement range can be increased comparing with the SBM technique. This technique has been successfully demonstrated by Ayubi *et al.* to generate better sinusoidal fringe patterns even with a smaller degree of defocusing [11].

### D. Optimal Pulse Width Modulation

We recently proposed OPWM to further improve the defocusing technique [12]. This technique selectively eliminates undesired frequency components by inserting different types of notches in a conventional binary square wave. Then, with a slightly defocused projector, ideal sinusoidal fringe patterns can be generated.

Figure 3 illustrates an OPWM pattern. The square wave is chopped $n$ times per half cycle. For a $2\pi$ periodic waveform, the Fourier series coefficients are

$$a_0 = \frac{1}{2\pi}\int_{\theta=0}^{2\pi} f(\theta)\mathrm{d}\theta = 0.5, \tag{8}$$

$$a_k = \frac{1}{\pi}\int_{\theta=0}^{2\pi} f(\theta)\cos(k\theta)\mathrm{d}\theta, \tag{9}$$

$$b_k = \frac{1}{\pi}\int_{\theta=0}^{2\pi} f(\theta)\sin(k\theta)\mathrm{d}\theta. \tag{10}$$

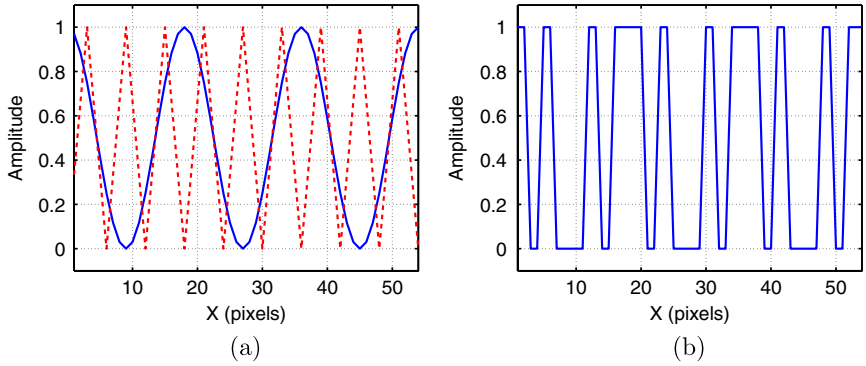


Fig. 2. (Color online) Modulate sinusoidal waveform with binary structured patterns. (a) The sinusoidal and the modulation waveforms. (b) The resultant binary waveform.

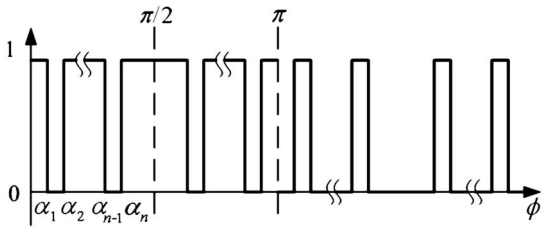

Fig. 3. Quarter-wave symmetric OPWM waveform.

Because of the half-cycle symmetry of the OPWM wave, only odd-order harmonics exist. Furthermore, $b_k$ can be simplified as

$$b_k = \frac{4}{\pi}\int_{\theta=0}^{2\pi} f(\theta)\sin(k\theta)\mathrm{d}\theta. \tag{11}$$

For the binary OPWM waveform, $f(\theta)$, we have

$$b_k = \frac{4}{\pi}\int_0^{\alpha_1}\sin(k\theta)\mathrm{d}\theta + \frac{4}{\pi}\int_{\alpha_2}^{\alpha_3}\sin(k\theta)\mathrm{d}\theta + \ldots + \frac{4}{\pi}\int_{\alpha_n}^{\pi/2}\sin(k\theta)\mathrm{d}\theta \tag{12}$$

$$= \frac{4}{k\pi}[1 - \cos k\alpha_1 + \cos k\alpha_2 - \cos k\alpha_3 + \ldots + \cos k\alpha_n]. \tag{13}$$

The $n$ notches in the waveform create $n$ degrees of freedom. It can eliminate $n-1$ number of selected harmonics while keeping the fundamental frequency component within a certain magnitude. To do this, one can set the corresponding coefficients in the above equation to be desired values (0 for the $n-1$ harmonics to be eliminated and the desired magnitude for the fundamental frequency), and solve for the angles for all notches [15]. For instance, to eliminate fifth, seventh, and 11th-order harmonics, two notches could be set, and the following equations could be formulated

$$b_1 = 1 - \cos(\alpha_1) + \cos(\alpha_2) - \cos(\alpha_3) + \cos(\alpha_4) = \pi/4, \tag{14}$$

$$b_5 = 1 - \cos(5\alpha_1) + \cos(5\alpha_2) - \cos(5\alpha_3) + \cos(5\alpha_4) = 0.0, \tag{15}$$

$$b_7 = 1 - \cos(7\alpha_1) + \cos(7\alpha_2) - \cos(7\alpha_3) + \cos(7\alpha_4) = 0.0, \tag{16}$$

$$b_{11} = 1 - \cos(11\alpha_1) + \cos(11\alpha_2) - \cos(11\alpha_3) + \cos(11\alpha_4) = 0.0. \tag{17}$$

The nonlinear equations require an optimization procedure to solve for the angles. Numerous research has been conducted on how to solve for this type of nonlinear equations. For example, some research has been conducted to solve for transcendental equations [16]. Because of the ability to eliminate undesired high-order harmonics, OPWM waveform could become sinusoidal after applying a low-pass filter, which is similar to a small degree of defocusing. Therefore, the depth measurement range can also be increased in comparison with the SBM technique.

Figure 4 shows the representative binary patterns for the SBM, SPWM, and OPWM. The fringe period is 60 pixels, SPWM modulation frequency is 6 pixels per period, and the OPWM is set to eliminate the fifth- and seventh-order harmonics.

### E. Phase Error Determination

For a 3D shape measurement technique based on fringe analysis, because the 3D information is retrieved from the phase, the measurement error is typically determined by the phase error under the same calibration circumstance. Therefore, evaluating one technique can be realized by finding the phase error caused by that technique.

It is important to note that it is very difficult for a real measurement system to find the phase error itself from the defocused binary patterns because the measured surface property may play a vital role, and the lens distortion complicates the problem. To circumvent this problem, we use three additional fringe patterns that are ideal sinusoidal fringe patterns with the same phase shift and the same number of pixels per fringe period. Therefore, for each measurement, we have four phase values, $\phi^s(x,y)$ from the ideal sinusoidal fringe pattern, $\phi^b(x,y)$ from the SBM patterns, $\phi^p(x,y)$ from the SPWM patterns, and $\phi^o(x,y)$ from the OPWM patterns. The phase errors are defined as the differences between the phase values obtained from the different methods and the phase from the ideal sinusoidal fringe patterns:

$$\Delta\phi^b(x,y) = [\phi^b(x,y) - \phi^s(x,y)] \mod 2\pi, \tag{18}$$

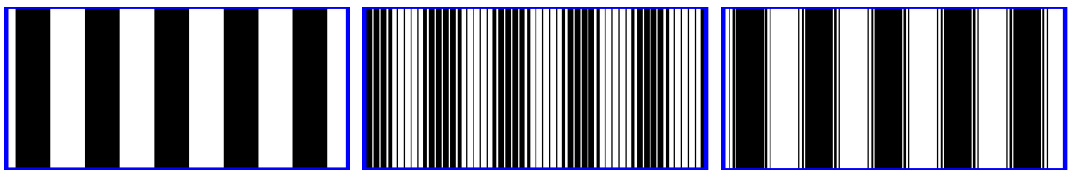

Fig. 4. (Color online) Example of three different patterns. (a) SBM pattern; (b) SPWM pattern; (c) OPWM pattern.

$$\Delta\phi^p(x,y) = [\phi^m(x,y) - \phi^s(x,y)] \mod 2\pi, \quad (19)$$

$$\Delta\phi^o(x,y) = [\phi^o(x,y) - \phi^s(x,y)] \mod 2\pi. \quad (20)$$

Here mod is the modulus operator. It should be noted that, theoretically, it does not need a modulus operation to obtain phase error from the wrapped phase since the patterns are perfectly aligned. However, due to camera sampling, the modulus operation is practically required to remove the 1-pixel $2\pi$ phase jump shift from the binary defocused phases to the sinusoidal phase.

### F. Influence of High-Order Harmonics on Phase

Since each harmonic will contribute to the profile of a binary structured pattern, it would be desirable to understand the influence of each harmonic's contribution to the phase error. The cross section of a squared binary structured pattern is a square wave; thus understanding the effect of a binary structured pattern can be simplified to the study of a square wave. A normalized square wave with a period of $2\pi$ can be written as

$$y(x) = \begin{cases} 0 & x \in [(2n-1)\pi, 2n\pi) \\ 1 & x \in [2n\pi, (2n+1)\pi) \end{cases}. \quad (21)$$

Here, $n$ is an integer number. The square wave can be expanded as a Fourier series:

$$y(x) = 0.5 + \sum_{k=0}^{\infty} \frac{2}{(2k+1)\pi} \sin[(2k+1)\pi]. \quad (22)$$

For a three-step phase-shifting algorithm with equal phase shift, our previous study [17] found that some high-order harmonics will not induce measurement errors. Specifically, we have demonstrated that the $3n$th-order harmonics will not influence phase error at all. If the high-order harmonics exist, the fringe patterns can be described as

$$I_1^h(x,y) = I'(x,y) + I''(x,y)\cos(\phi - 2\pi/3) + \ldots I_k(x,y)\cos[(2k+1)(\phi - 2\pi/3)], \quad (23)$$

$$I_2^h(x,y) = I'(x,y) + I''(x,y)\cos(\phi) + \ldots I_k(x,y)\cos[(2k+1)\phi], \quad (24)$$

$$I_3^h(x,y) = I'(x,y) + I''(x,y)\cos(\phi + 2\pi/3) + \ldots I_k(x,y)\cos[(2k+1)(\phi + 2\pi/3)], \quad (25)$$

where $k = 1, 2, 3, \ldots$ are integers in Eq. (22). When just the $3n$th-order harmonics exist (i.e., third, ninth), Eq. (4) can be rewritten as

$$\phi(x,y) = \tan^{-1}[\sqrt{3}(I_1^h - I_3^h)/(2I_2^h - I_1^h - I_3^h)] \quad (26)$$

$$= \tan^{-1}[\sqrt{3}(I_1 - I_3)/(2I_2 - I_1 - I_3)]. \quad (27)$$

From this equation, we can see that what matters is the difference values of $I_1 - I_3$ and $2I_2 - I_1 - I_3$. It is clear that when the $3n$th-order harmonics exist, the differences do not change, and no phase error will be introduced. Therefore, these harmonics do not need to be accounted to improve the measurement quality.

## 3. Optimization Criteria

### A. SPWM

The difference between SBM and SPWM is that SPWM utilizes a higher-frequency ($f_c$) triangular wave to modulate the ideal sinusoidal wave, shifting the higher-order frequency harmonics further away from the fundamental frequency $f_0$. The only variable is the modulation frequency $f_c$. Therefore, the goal of SPWM optimization is to find an optimal modulation frequency $f_c^o$ so that the measurement quality will be the best under all circumstances, i.e., different amounts of defocusing for different fundamental frequencies. In addition, to maintain the fundamental difference between SPWM and SBM, the modulation frequency must be much higher than the fundamental frequency, i.e., $f_c > f_0$. The performance is evaluated based upon the criteria of the introduced phase error instead of the sinusoidality appearance.

### B. OPWM

Because the OPWM technique has the ability to selectively eliminate high-order harmonics, it provides more flexibility to control the pattern structure, while complicating the problem. The solution to the nonlinear equation set is essentially a nonlinear optimization problem, which often leads to multiple solutions. However, as addressed in Subsection 2.F., for a three-step phase-shifting algorithm with equal phase shift, we only need to eliminate the high-order harmonics except those $3n$th-order ones. This simplifies the problem since there are fewer harmonics to consider.

In other words, the most dominant phase error is caused by fifth- and seventh-order harmonics. Therefore, if we could remove these two frequency components, the measurement error should be very small since the next harmonics introducing the phase error is the 11th order. For the defocusing technique, it is quite easy to suppress the 11th order and above harmonics by slightly defocusing the projector.

## 4. Simulations

### A. Simulation on Influence of High-Order Harmonics

Our first simulation is to verify the influence of high-order harmonics on phase error. This simulation was carried out by analyzing the phase error introduced by each frequency harmonics. Equation (22) indicates that the magnitudes of high-order harmonics

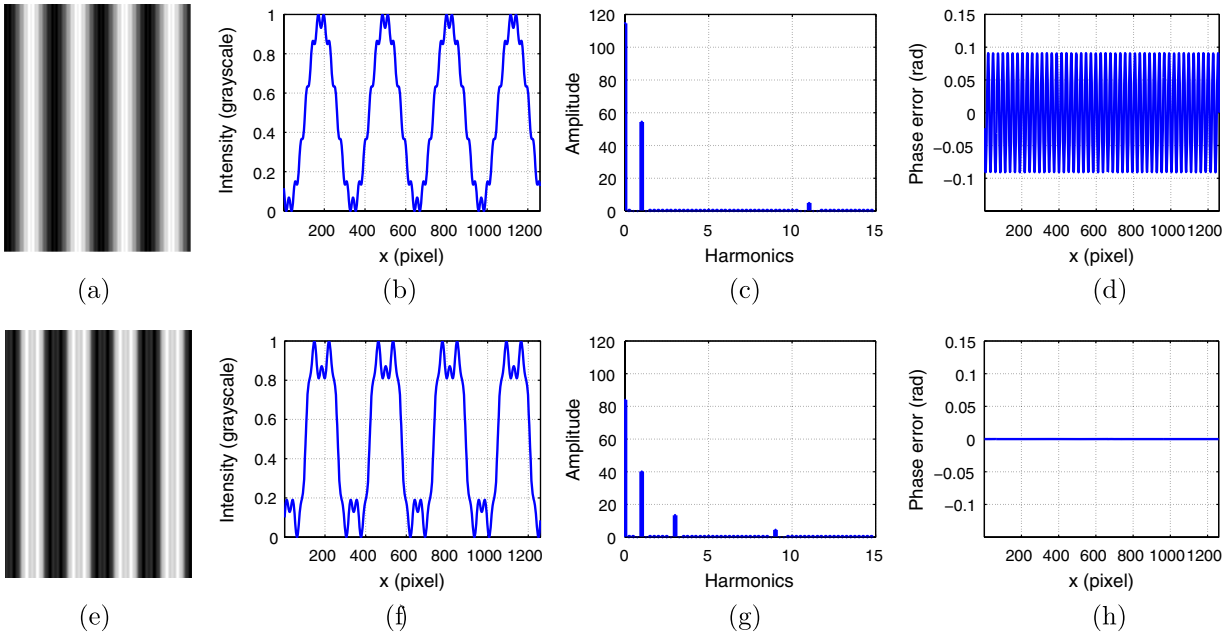


Fig. 5. (Color online) Influence of high-order harmonics on phase error. (a) Fringe pattern containing + 11th-order harmonics components. (b) Cross-section of (a). (c) Frequency spectrum of (b). (d) Phase error for signal in (b); (e)–(h) The corresponding results when the signal includes the fundamental, third, and ninth-order harmonics.

decrease gradually. This means that when the order is very high (e.g., higher than 11th order), its induced error could be negligible.

To demonstrate this, we firstly determine the theoretical phase error on each harmonics. The phase error was determined by combining the fundamental frequency with only one higher-order component, i.e., the signal can be described as

$$I^k(x,y) = 0.5 + \frac{2}{3\pi}\sin(f_0 x) + \frac{2}{(2k+1)\pi}\sin[(2k+1)f_0 x]. \quad (28)$$

A three-step phase-shifting with equal phase shift was used to determine the phase, and the associated phase error was calculated by comparing against the ideal one. Figure 5 shows the influence of each individual harmonic on phase error. This confirms that no phase error is introduced by $3n$th-order harmonics, and the phase error decreases when the other harmonic order increases. This indicates that it is not sufficient to look at the appearance of fringe patterns nor their frequency spectra [18]. Example in Fig. 5 clearly shows that the less sinusoidal patterns could have less phase errors (thus better measurement quality) than those seemingly better sinusoidal patterns.

### B. Simulation on SPWM Optimization

The defocusing effect can be approximated as a Gaussian smoothing filter. A 2D Gaussian filter is usually defined as

$$G(x,y) = \frac{1}{2\pi\sigma^2} e^{-\frac{(x-\bar{x})^2+(y-\bar{y})^2}{2\sigma^2}}. \quad (29)$$

Here $\sigma$ is standard deviation and $\bar{x}$ and $\bar{y}$ are mean values of the $x$ and $y$ axis, respectively.

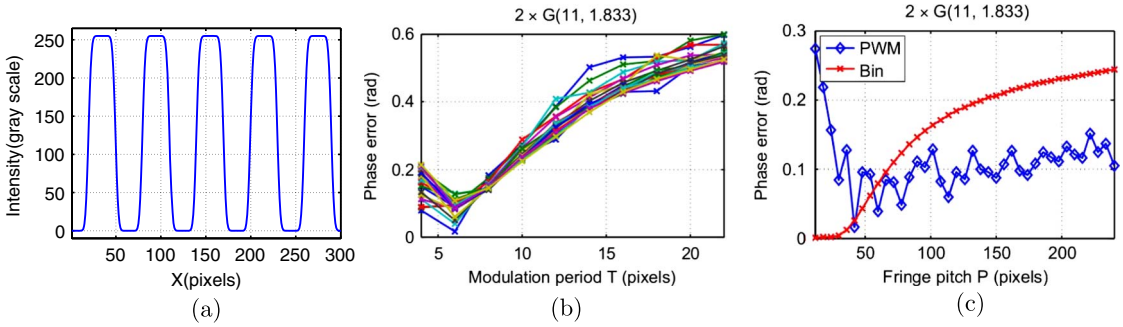


Fig. 6. (Color online) Influence of modulation frequency and fringe pitch on phase error with a nearly focused projector. (a) The square binary pattern after defocusing. (b) Phase error changes with modulation frequencies for different fringe pitches ($P = 36 + 6 \times n$, $n = 1, 2, \ldots 10$). (c) Phase error changes with the fringe pitches $P$ (modulation period $T = 6$ pixels).

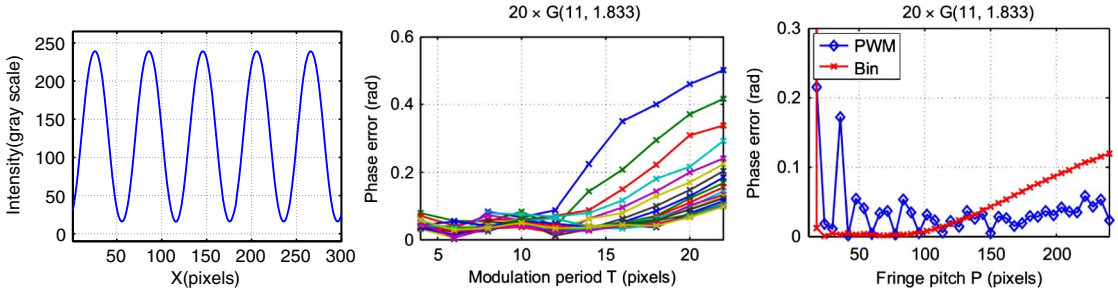


(a) (b) (c)

Fig. 7. (Color online) Influence of modulation frequency and fringe pitch on phase error with a significantly defocused projector. (a) The square binary pattern after defocusing. (b) Phase error changes with modulation frequencies for different fringe pitches ($P = 36 + 6 \times n$, $n = 1, 2, \ldots 10$). (c) Phase error changes with the fringe pitches $P$ (modulation period $T = 6$ pixels).

For our case, because the structured stripes are either vertical or horizontal, only one cross section perpendicular to the fringe stripes needs to be considered, which means the problem is reduced to 1D. A 1D Gaussian filter is defined as

$$G(x) = \frac{1}{\sqrt{2\pi}\sigma} e^{-\frac{(x-\bar{x})^2}{2\sigma^2}}. \tag{30}$$

We first simulate the defocusing effect by applying a Gaussian filter to the signal. The degree of defocusing can be represented as the breadth of the Gaussian filter that is determined by the standard deviation and the filter size. We applied a small Gaussian filter with size of 11 and standard deviation of 1.83 pixels twice to emulate that the nearly focused case. Figure 6(a) shows the square binary pattern after applying the filter. It can be seen that the binary structure is very clear, which emulates the pattern generated by a nearly focused projector. In the simulation shown in Fig. 6(b), we determined how the modulation frequency affects the measurement error for different fringe pitches, $P$, the number of pixels per fringe period. To minimize the digital effect on phase shift and binarization, an increment of 6 pixels is used for the binary patterns, and an increment of 2 pixels is used for the modulation pulse width to ensure the symmetry of a triangular waveform. The fringe pitch $P$ starts with 42 pixels because when it is very small, the error appears random (mainly because of the digital effect). This simulation result shows that when the modulation pulse width is 6 pixels, the phase error for almost all the fringe pitches at their valley points, meaning that 6 pixel modulation frequency period could be the optimal one to use.

Another simulation was carried out to determine whether the SPWM technique can improve the quality of 3D shape measurement by reducing measurement error. Figure 6(c) shows the results. This

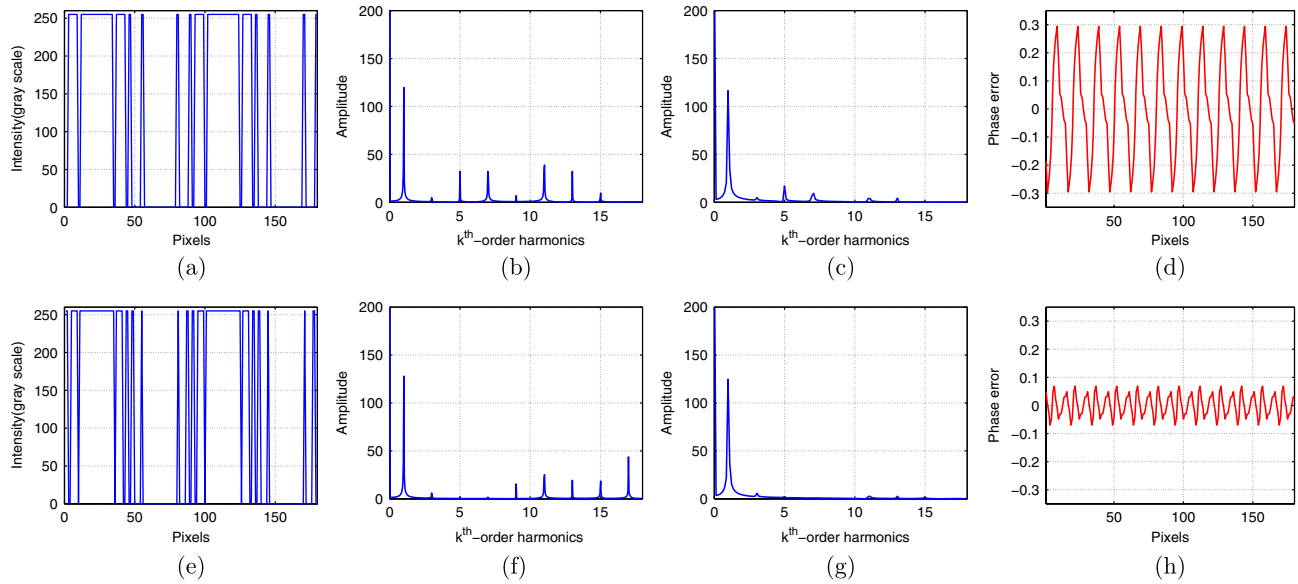


(a) (b) (c) (d)

(e) (f) (g) (h)

Fig. 8. (Color online) OPWM optimization example. The first row shows a bad OPWM pattern, and the second row shows the good OPWM pattern. (a) One of the three phase-shifted OPWM patterns. (b) The frequency spectra before smoothing. (c) The frequency spectra after applying a smoothing filter. (d) The phase error. (e) One of the three phase-shifted OPWM patterns. (f) The frequency spectra before smoothing. (g) The frequency spectra after applying a smoothing filter. (h) The phase error.

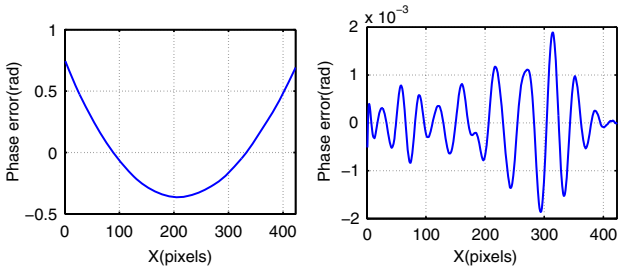


Fig. 9. (Color online) Validation of the ideal sinusoidal fringe patterns utilized as reference. (a) The unwrapped phase map. (b) The actual phase error that will be coupled into the real measurement.

simulation is to compare the phase error between the original binary patterns and the SPWM patterns under the same condition with different fringe pitches. Again the SPWM period $T$ was chosen to be 6 pixels to minimize the error. This simulation shows that when the fringe pitch is larger than 56, the modulated patterns give smaller phase error. However, when the fringe pitch is small, the original squared binary pattern actually works better. One interesting thing to notice is that when the period of fringe patterns increases, the phase error does not significantly increase for the SPWM technique.

We then applied the same Gaussian filter 20 times to represent the significantly defocused cases. The corresponding results are shown in Fig. 7. This simulation shows that when the patterns are significantly defocused, a modulation period of 6 pixels still gives close to the minimum errors for different frequency of fringe patterns, while between 6 and 12 pixels, the results are decent. However, in comparison with the phase error for the traditional binary method, only after the fringe pitch increases to a certain level, this SPWM method will perform better.

Finding the optimal pulse width to minimize the phase error should be the criteria for evaluating the performance of different patterns. This simulation results show that: (1) the SPWM technique actually deteriorates the measurement quality if the fringe pitch is smaller than a certain number; (2) the optimal modulation period is consistently 6 pixels if the projector is nearly focused; and (3) the optimal modulation period ranges 6–10 pixels if the projector is significantly defocused.

### C. Simulation on OPWM optimization

The simulation presented in Section 4.A. shows that $3n$th-order harmonics do not introduce any phase error for a three-step phase-shifting algorithm with equal phase shift. Therefore, these frequency components should not be considered during the optimization procedure. In other words, although the third-order harmonics have more influence on the square wave than the fifth and seventh, we do not need to consider its influence on our measurement accuracy.

Figure 8(a) and 8(e) show two different OPWM patterns with a fringe pitch of 90 pixels. Figures. 8(b) and 8(f) show their corresponding frequency spectra. It clearly shows that Fig. 8(f) has smaller fifth and seventh harmonics magnitudes than those shown in Fig. 8(b); therefore, its performance should be better. These patterns were then smoothed by a Gaussian filter (size of 11 with a standard deviation

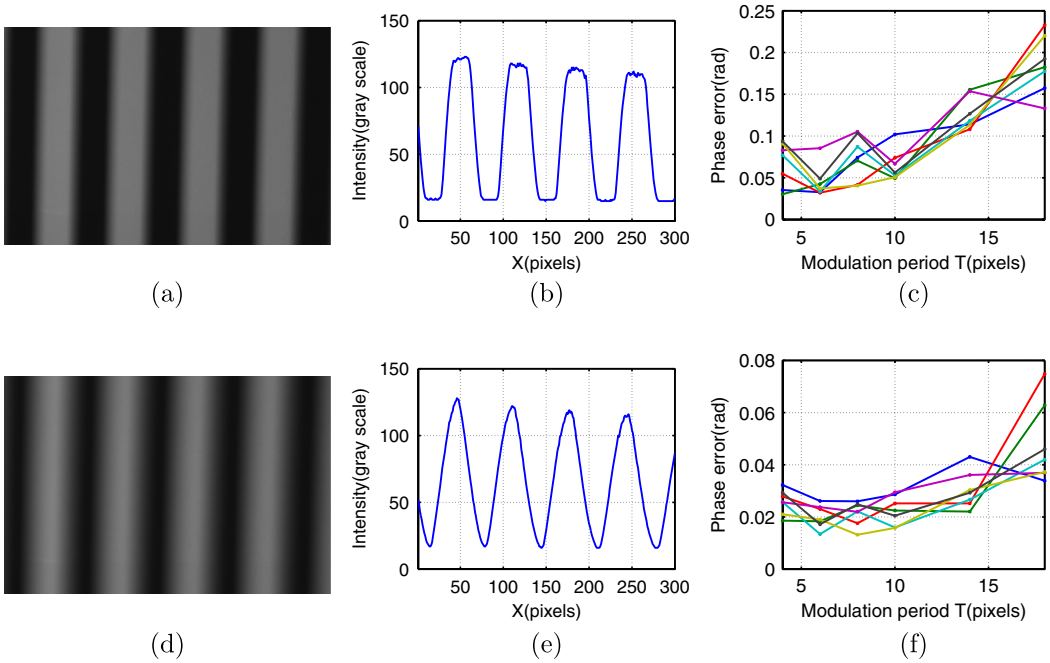


Fig. 10. (Color online) Experimental results on modulation frequency selections. The fringe pitches used here are 42, 60, 72, 90, 102, and 150 pixels. (a) The binary square pattern when the projector is nearly focused. (b) The cross section of (a). (c) The results when the projector is nearly focused; (d)–(f) show the corresponding results when the projector is significantly defocused.

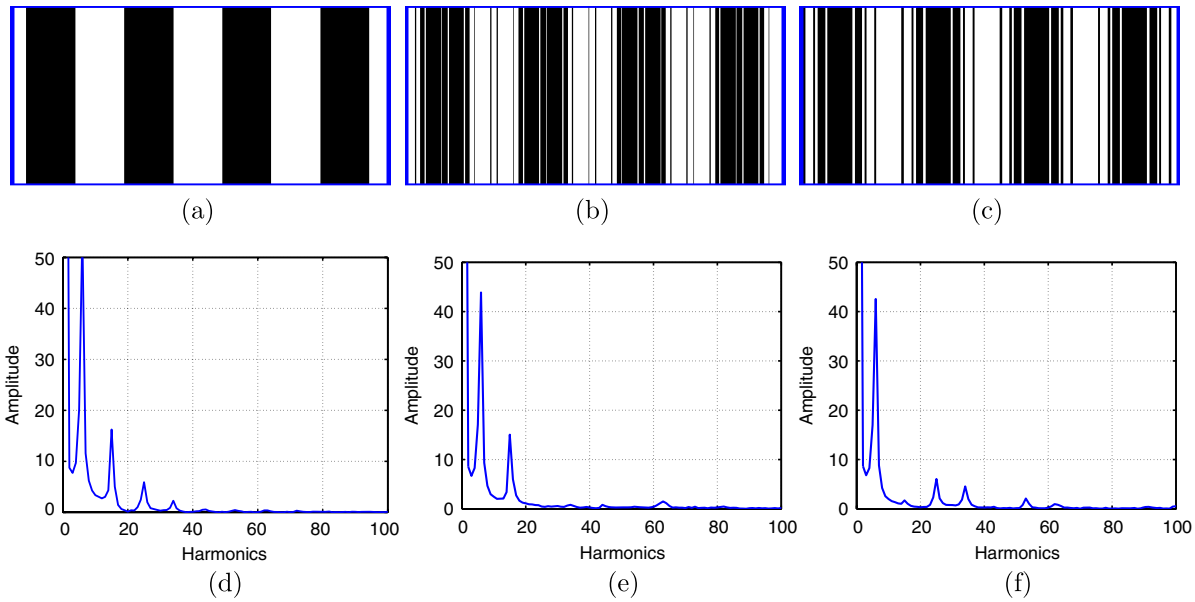


Fig. 11. (Color online) OPWM optimization results. (a) The SBM pattern with 90 pixels per period. (b) OPWM pattern with third-order harmonics but without fifth- or seventh-order harmonics. (c) OPWM pattern with fifth- and seventh-order harmonics but without third-order harmonics. (d) Frequency spectra of the SBM pattern shown in (a). (e) Frequency spectra of the OPWM pattern in (b). (f) Frequency spectra of the OPWM pattern shown in (c).

of 5 pixels). Figures 8(c) and 8(g) show the Fourier spectra after applying the smoothing filter. Most of the high-order harmonics were completely suppressed by the smoothing filter for the better designed OPWM pattern shown in Fig. 8(e). Finally, the phase errors shown in Figs. 8(d) and 8(h) confirm that if the fifth and seventh harmonics are well eliminated, the phase error would be very small.

## 5. Experiments

### A. Experimental System Setup

Experiments were also performed to verify the simulation results. In this research, we used a digital-light-processing projector (Model: Samsung SP-P310MEMX) and a digital CCD camera (Model: Jai Pulnix TM-6740CL). The camera uses a 16 mm focal length Mega-pixel lens (Model: Computar M1614-MP) at $F/1.4$ to 16C. The camera resolution is 640 × 480 with a maximum frame rate of 200 frames/sec. The camera pixel size is $7.4 \times 7.4\ \mu m^2$. The projector has a resolution of 800 × 600 with a projection distance of 0.49–2.80 m.

### B. Validation of Ideal Sinusoidal Fringe Pattern Generation

This experiment is to verify that the adopted conventional sinusoidal method does not bring significant phase error, since we used the phase obtained from these patterns as our reference. In the experiments, a uniform white plate was used to quantitatively show the introduced phase errors by this method. Since the projector is a nonlinear device, the projection nonlinearity needs to be corrected. In this research, we used the method proposed in [4] to actively change the patterns before projection. Figure 9(a) shows one cross section of the unwrapped phase map. The larger profile was introduced by 3D shape measurement system (e.g., lens distortions, board flatness). The general profile will not introduce additional phase error since it is systematically caused by the hardware system, rather than the fringe quality. The phase error was obtained by removing the general profile of the unwrapped phase, which is shown in Fig. 9(b). It can be seen that the projection nonlinear influence was effectively alleviated and the introduced random error is negligible in comparison with the digitization error.

### C. Validation of Optimal Modulation Frequency Selection for SPWM

The optimal modulation frequency determined from Section 4 was then validated by experiments. Figure 10(a) shows the square binary pattern when the projector is nearly focused and Fig. 10(b) shows the cross section. Figure 10(c) shows the experimental

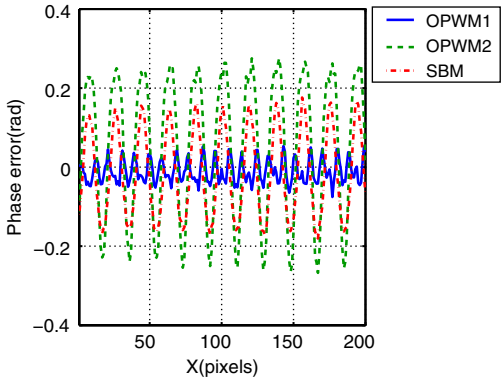


Fig. 12. (Color online) Phase errors from the SBM pattern and different OPWM patterns.

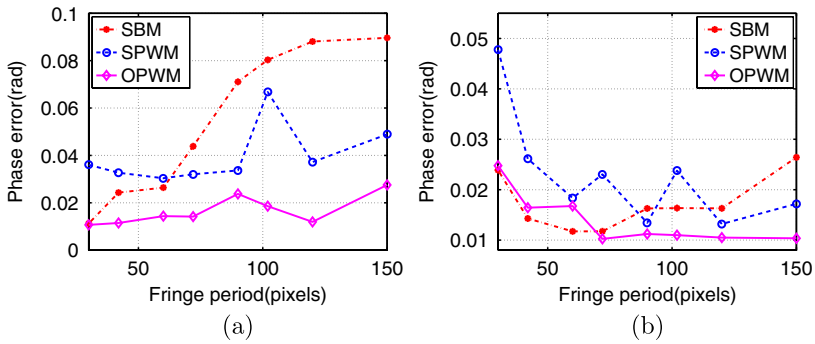


Fig. 13. (Color online) Comparisons among SBM, SPWM, and OPWM under their respective optimal conditions. (a) The projector is nearly focused. (b) The projector is significantly defocused.

results for SPWM patterns with different pitches when the projector is nearly focused. It indeed verifies that in most cases, the optimal modulation period is 6 pixels. When the projector is significantly defocused, the corresponding results are shown in Fig. 10(d)–10(f). Again, it agrees with our simulation very well: the optimal modulation period ranges 6–10 pixels.

### D. Validation of OPWM

To verify the performance of different OPWM patterns, we designed two different OPWM patterns to compare with the SBM patterns. Figure 11(a) shows the SBM pattern and the Fourier spectra of the cross section is shown in Fig. 11(d). Figure 11(b) shows the OPWM patterns with fifth and seventh-order harmonics well eliminated but with the third-order harmonics, and its Fourier spectra is shown in Fig. 11(e). Figure 11(c) shows another OPWM pattern with third-order harmonics eliminated but keeping the fifth- and seventh-order harmonics, and Fig. 11(f) shows its Fourier spectra. The phase errors of these three sets of patterns are shown in Fig. 12. From this experiment, we can see that the

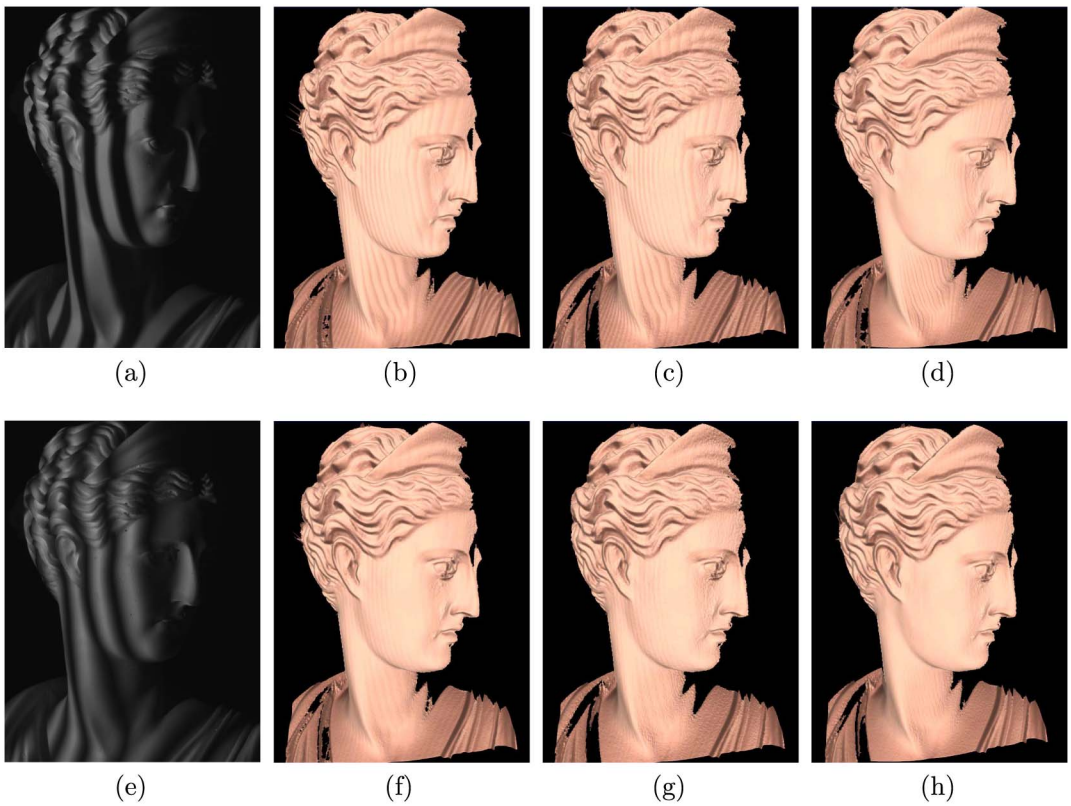


Fig. 14. (Color online) 3D complex shape measurement under different amounts of defocusing. The first row shows the result when the projector is nearly focused, and the second row shows the results when the projector is significantly defocused. (a) Binary pattern when projector is nearly focused. (b) 3D result using SBM patterns. (c) 3D result using SPWM patterns. (d) 3D result using OPWM patterns. (e) Binary pattern when projector is more defocused. (f) 3D result using SBM patterns. (g) 3D result using SPWM patterns. (h) 3D result using OPWM patterns.

fifth and seventh harmonics could cause severe phase errors. On the other hand, the phase error is really small when the magnitude of the third-order harmonic is very large. This finding matches well with our simulation. This means if those undesired harmonics are well eliminated, the phase errors will become small enough for measurement. However, this experiment also shows that if the OPWM pattern (as shown in the OPWM pattern 2) was poorly designed, it could drastically deteriorate the measurement quality.

### E. Comparison among SBM, SPWM, and OPWM

Experiments were also carried out to compare the performance of different techniques under their respective optimal conditions. In this set of experiments, again we considered two cases, the nearly focused projector and the significantly defocused projector. The SPWM and OPWM patterns were optimized according to the findings discussed above. Figure 13(a) shows the error comparison results with a nearly focused projector. Figure 13(b) shows the results when the projector is significantly defocused. From these experiments, we can see that when the projector is nearly focused, the OPWM performs the best while the SPWM performs better than SBM if the fringe pitch is large. When the projector is significantly defocused, the SBM performs similarly as the OPWM technique when the fringe is dense, while the SBM performs the worst when the fringe stripe is very wide.

### F. Complex Shape Measurement

Additional experiments were conducted to measure complex 3D shape using these techniques and to compare their performance visually. In this experiment, we used $P = 60$ pixels fringe patterns for all three methods and performed the measurement when the projector is nearly focused and significantly defocused. Figure 14(a) shows one of the fringe patterns for the SBM patterns when the projector is nearly focused; it clearly shows the binary structure. Figures 14(b)–14(d) respectively show the reconstructed 3D results from SBM, SPWM, and OPWM patterns when the projector is nearly focused. This experiment indeed shows that the SPWM performs better than the SBM, while the OPWM performs the best.

Figure 14(e) shows one of the fringe patterns for the SBM patterns when the projector is significantly defocused, and the patterns are close to being sinusoidal. 3D shape measurement results under this degree of defocusing are shown in Figs. 14(f)–14(h). Under this condition, all methods, as expected, result in reasonable good-quality 3D shape measurement, with the OPWM delivering the best result again. It should be noted that this system was calibrated using the reference-plane based method described in [19], and the phase was unwrapped using the quality-guided phase-unwrapping algorithm presented in [20]. Even though the calibration method used is not very accurate, it helps to present the 3D data for visual comparison.

## 6. Conclusion

This paper has presented some comparisons among the recently proposed three binary defocusing techniques: SBM, SPWM, and OPWM. To achieve this, different breaths of fringe patterns were projected for test. The projector was set to be nearly focused and be significantly defocused. The phase errors were obtained by comparing phase maps from those three patterns with sinusoidal pattern. In this paper, the optimization for designing SPWM and OPWM patterns were also presented. Finally, our experiments have found that: (1) the OPWM performs the best if it was well optimized, (2) the SBM performs well when the fringe stripe is narrow or the projector is well defocused, and (3) the SPWM performs better than the SBM in most cases when the fringe stripe is wide enough. We hope this presentation would be helpful for those who would like to use the binary defocusing techniques for 3D shape measurement, as this paper can guide them to select the proper method under their measurement conditions.

The authors would like to thank Leah Merner for her proofreading this paper.

## References

1. S. Gorthi and P. Rastogi, "Fringe projection techniques: Whither we are?" Opt. Lasers Eng. **48**, 133–140 (2010).
2. X. Su and Q. Zhang, "Dynamic 3D shape measurement method: A review," Opt. Lasers Eng. **48**, 191–204 (2010).
3. Q. Zhang and X. Su, "High-speed optical measurement for the drumhead vibration," Opt. Express **13**, 3110–3116 (2005).
4. C. Zhang, P. S. Huang, and F.-P. Chiang, "Microscopic phase-shifting profilometry based on digital micromirror device technology," Appl. Opt. **41**, 5896–5904 (2002).
5. B. Pan, Q. Kemao, L. Huang, and A. Asundi, "Phase error analysis and compensation for nonsinusoidal waveforms in phase-shifting digital fringe projection profilometry," Opt. Lett. **34**, 416–418 (2009).
6. H. Guo, H. He, and M. Chen, "Gamma correction for digital fringe projection profilometry," Appl. Opt. **43**, 2906–2914 (2004).
7. S. Zhang and P. S. Huang, "Phase error compensation for a three-dimensional shape measurement system based on the phase shifting method," Opt. Eng. **46**, 063601 (2007).
8. K. Liu, Y. Wang, D. L. Lau, Q. Hao, and L. G. Hassebrook, "Gamma model and its analysis for phase measuring profilometry," J. Opt. Soc. Am. A **27**, 553–562 (2010).
9. S. Zhang and S.-T. Yau, "Generic nonsinusoidal phase error correction for three-dimensional shape measurement using a digital video projector," Appl. Opt. **46**, 36–43 (2007).
10. S. Lei and S. Zhang, "Flexible 3-D shape measurement using projector defocusing," Opt. Lett. **34** (20), 3080–3082 (2009).
11. G. A. Ajubi, J. A. Ayubi, J. M. D. Martino, and J. A. Ferrari, "Pulse-width modulation in defocused 3-D fringe projection," Opt. Lett. **35**, 3682–3684 (2010).
12. Y. Wang and S. Zhang, "Optimum pulse width modulation for 3-D shape measurement with projector defocusing," Opt. Lett. **35**, 4121–4123 (2010).
13. D. Malacara, ed., *Optical Shop Testing*, 3rd ed. (Wiley, 2007).
14. Y. Xu, L. Ekstrand, J. Dai, and S. Zhang, "Phase error compensation for 3-D shape measurement with projector defocusing," Appl. Opt. **50**, 2572–2581 (2011).
15. V. G. Agelidis, A. Balouktsis, and I. Balouktsis, "On applying a minimization technique to the harmonic elimination PWM

control: The bipolar waveform," IEEE Power Electron. Lett. **2**, 41–44 (2004).
16. J. N. Chiasson, L. M. Tolbert, K. J. Mckenzie, and Z. Du, "A complete solution to the harmonics elimination problem," IEEE Trans. Power Electron. **19**, 491–499 (2004).
17. S. Zhang, "High-resolution 3-D profilometry with binary phase-shifting methods," Appl. Opt. **50**, 1753–1757 (2011).
18. Y. Wang and S. Zhang, "Optimal pulse width modulation for sinusoidal fringe generation with projector defocusing: Reply to comments," Opt. Lett. **36**, 809 (2011).
19. S. Zhang, D. van der Weide, and J. Olvier, "Superfast phase-shifting method for 3-D shape measurement," Opt. Express **18**, 9684–9689 (2010).
20. S. Zhang, X. Li, and S.-T. Yau, "Multilevel quality-guided phase unwrapping algorithm for real-time 3-D shape reconstruction," Appl. Opt. **46**, 50–57 (2007).